Proceedings of the Institute of Acoustics

SMALL OBJECT DETECTION WITH A DUAL-FREQUENCY SYNTHETIC APERTURE SONAR

John E Piper Naval Surface Warfare Center, Panama City, Florida, USA
Raymond Lim Naval Surface Warfare Center, Panama City, Florida, USA

1 INTRODUCTION

A Small Synthetic Aperture Minehunter (SSAM) has recently been acquired by the Naval Surface Warfare Center, Panama City. This autonomous underwater vehicle (AUV) is based on a REMUS 600 developed by Woods Hole Oceanographic Institute. It typically operates at 1.5 m/s and has mission times of several hours. Figure 1 shows a picture of SSAM. An extra set of triaxial fins can be seen mounted forward. These have allowed excellent vehicle control and stability for synthetic aperture work.

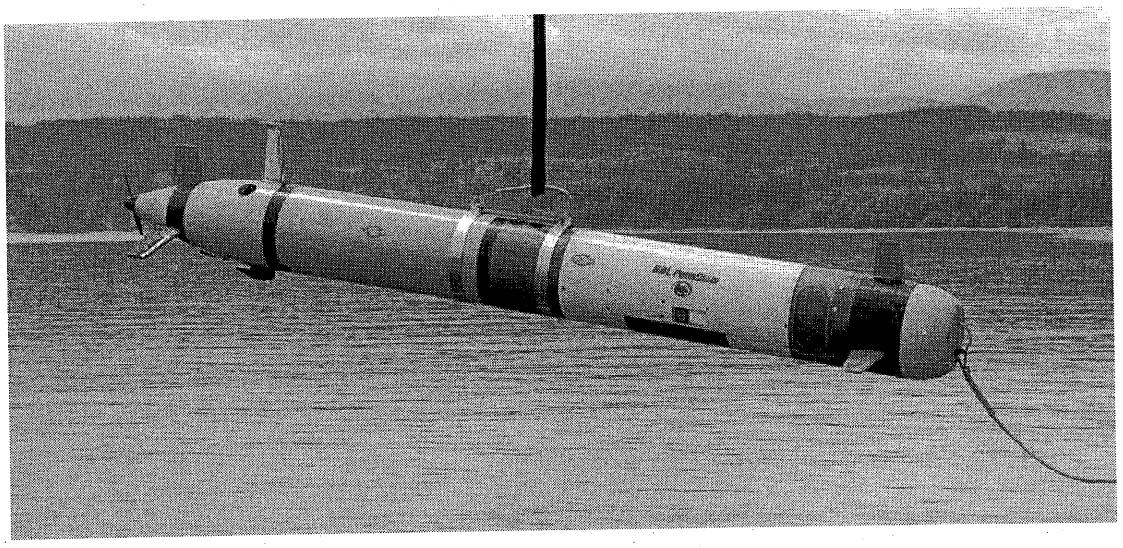

Fig. 1. Small Synthetic Aperture Minehunter (SSAM)

Experience has shown that dual-frequency sonar systems are complimentary when trying to detect objects. Generally, the high frequency (HF) sonar produces finer resolution, while the lower frequency (LF) sonar often has effectively stronger interactions for partially and fully-buried objects[1]. SSAM has both port and starboard 8-element arrays for a 105-135 kHz high frequency sonar and a 10-55 kHz broadband sonar.

This paper investigates SSAM's detection performance against small proud, partially-buried and fully-buried cylinders and uses the processed imagery to assess and validate simulations performed with recent upgrades to NSWC PC's PCSWAT[2] sonar performance software. The upgrades in

question enable performance simulations against targets subject to various degrees of burial and account for potential effects due to bottom ripple.

2 SERDP TEST FIELD

The cylindrical targets used in this test approximated the sizes of small unexploded ordinance (UXO). Four sizes were used in the test field: 5x25 cm (A), 7.5x35 cm (B), 10x50 cm (C), and 15x70 cm (D). They were constructed from steel, filled with Quikrete, and had an eyebolt on one end attached to a buried screw anchor with parachute cord.

Three of each target size were deployed off Panama City in a line with one target flush buried, another target half buried, and the last target proud. The field was in about 18 m of water and was somewhat disturbed by large swells generated by Hurricane Katrina. This resulted in classic scouring patterns around the targets and uncovering of at least one of the buried targets (A). Pictures of the four half-buried targets taken just before the test are shown in figure 2.

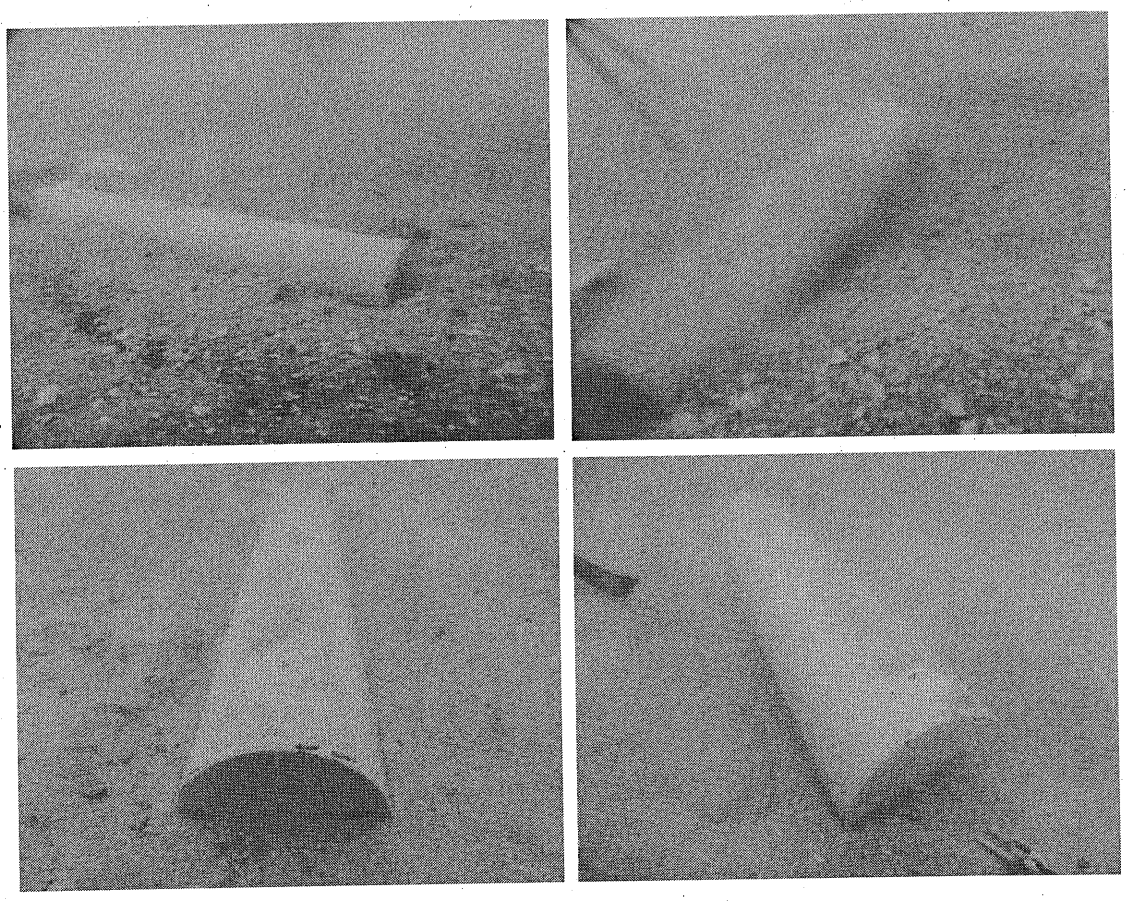

Fig. 2. The four half-buried targets in field.

The field generally had a good ripple pattern with 80-cm spacing as seen in figure 3. The targets would generally tend to orient themselves between the ripples. Figure 4 shows that in some sections of the target field the ripples were more irregular with 50 to 60-cm spacing and that features resembling moguls with dimensions of 1 to 2 m can also be seen. These physical dimensions can potentially hide the smaller targets in their acoustic shadow. The dimensions are also important parameters for models that predict subcritical detection of buried targets.

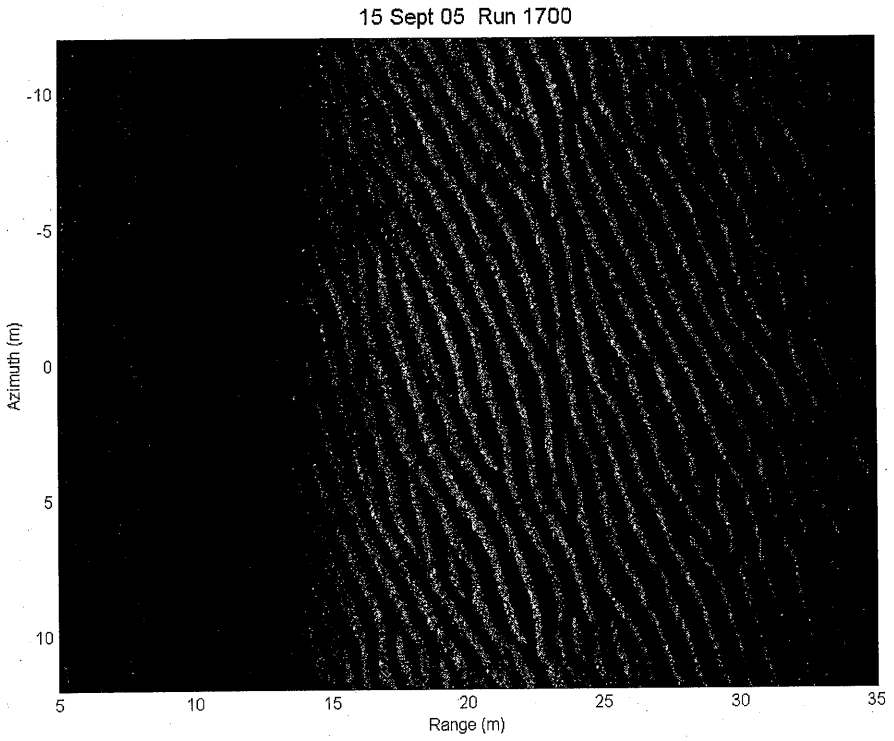

Fig. 3. Sand ripples with 80-cm wavelength. Beampattern effects can be seen at shorter ranges.

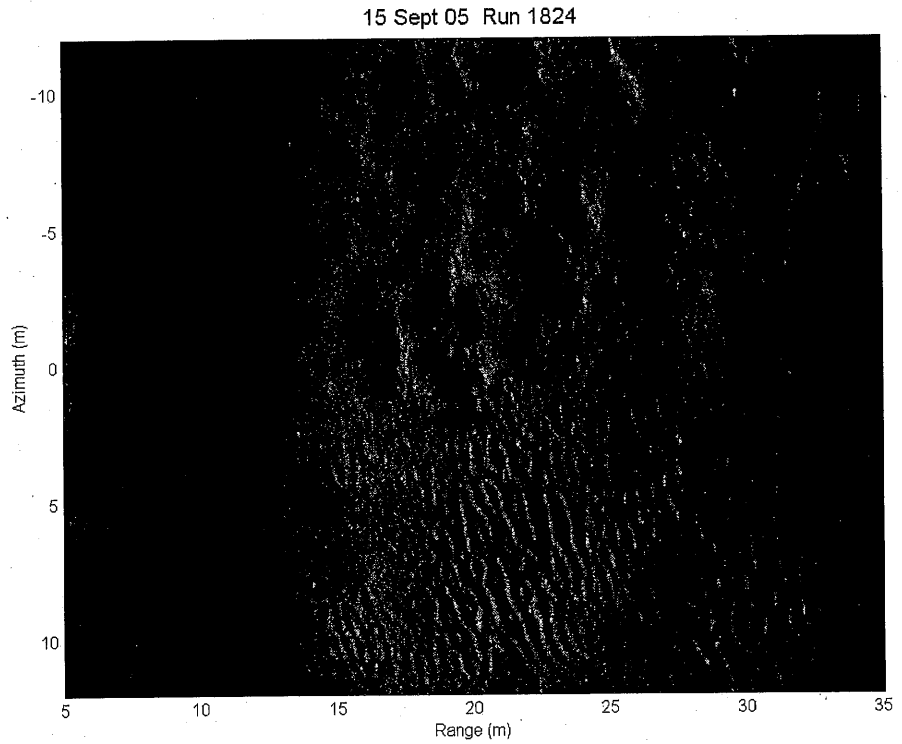

Fig. 4. Irregular sand ripples with 50 to 60-cm wavelength and 1 to 2-m moguls.

3 DATA PROCESSING

SSAM collected data from the SERDP field from the 13th to the 16th of September 2005. Processing the data occurred in three steps; preprocessing, motion compensation, and beamforming.

The preprocessor essentially reads a user specified block of raw pings and performs a pulse compression using a matched filter. For the 1.67-msec 105 to 135-kHz LFM signal, this results in a 2.5-cm resolution pulse compressed signal. For the 2-msec 10 to 55-kHz LFM signal, this results in a 1.6-cm resolution pulse compressed signal.

Fortunately, due to the stability of SSAM, motion compensation corrections are typically small. Motion is estimated using a two-element overlap in the ping rate. This overlap is used to accurately estimate the displaced phase center offset distance. The onboard Kearfott IMU data is also used to estimate the motion. The heading estimate is typically the most important parameter from the IMU. These combined estimates are then used to construct a track. A Hessian normal fit from the first to the last phase center then yields the motion correction vector. An example corresponding to the image in figure 3 is shown in figure 5. It should be noted that over the 30-m aperture of this track the maximum correction was only a little over 1 cm. In general, the overall stability of SSAM allows it to consistently produce good, well-focused images with only small motion compensation corrections.

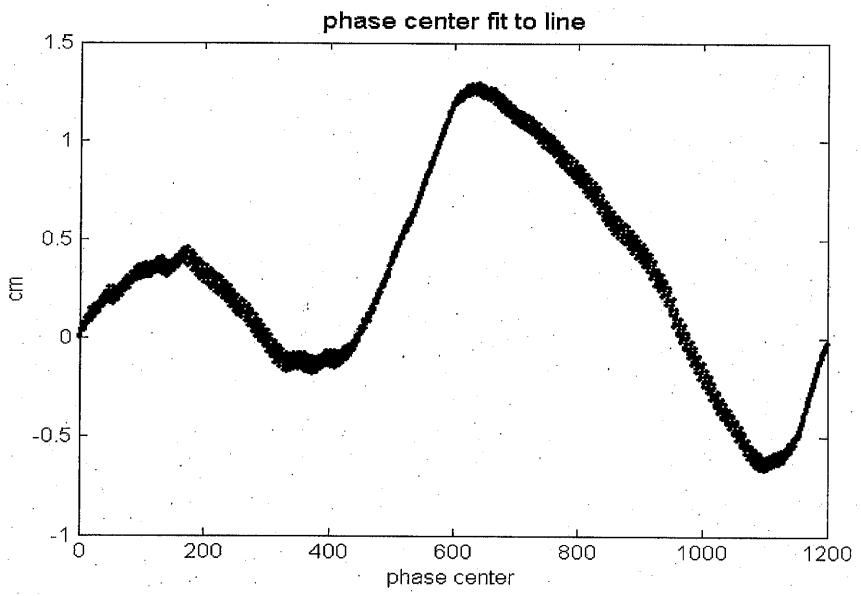

Fig. 5. Motion compensation correction vector.

The synthetic aperture beamformer is based on a wavenumber algorithm. This has the advantage of being faster than time-delay beamformers. A general description of this algorithm can be found elsewhere[2]. For this experiment the high frequency data was processed with 2.5x2.5-cm pixel resolution, and the broadband data was processed with 5x1.25-cm pixel resolution.

4 RESULTS

SSAM had good detections of all the targets, except the smallest buried target (A). The divers found that this target was only 80-90% buried but missed getting its location coordinates. Without this information, and given how small and buried it was, a confident detection could not be called. Otherwise, multiple detections of all the targets were made with typical detections between 25 and 40 dB.

The detection results are aspect dependent with the best aspects being end-on or broadside. Figure 6 shows the high frequency and broadband images of an end-on 10x50-cm cylinder. This target was about 60% buried and yielded a 35.6-dB SNR for the high frequency detection and a 35.2-dB SNR for the broadband detection for the front end-on aspect. The far end of this target had an eyebolt, which was attached to a buried screw anchor with parachute cord. Additionally, the targets were interconnected with parachute cord that is visible in the high frequency image as a vertical line that goes by the far end of the cylinder.

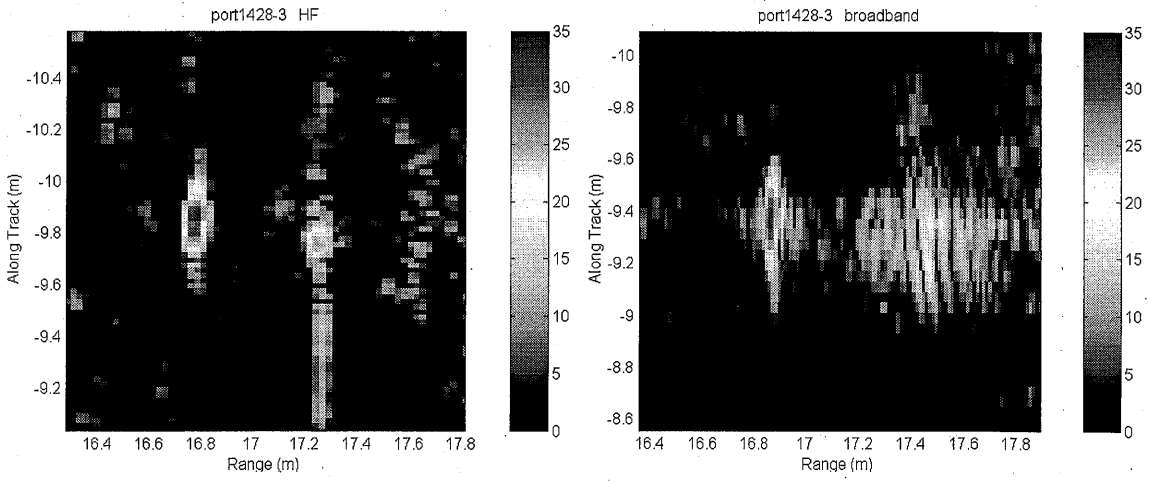

Fig. 6. High frequency and broadband end-on images of 60% buried 10x50-cm cylinder.

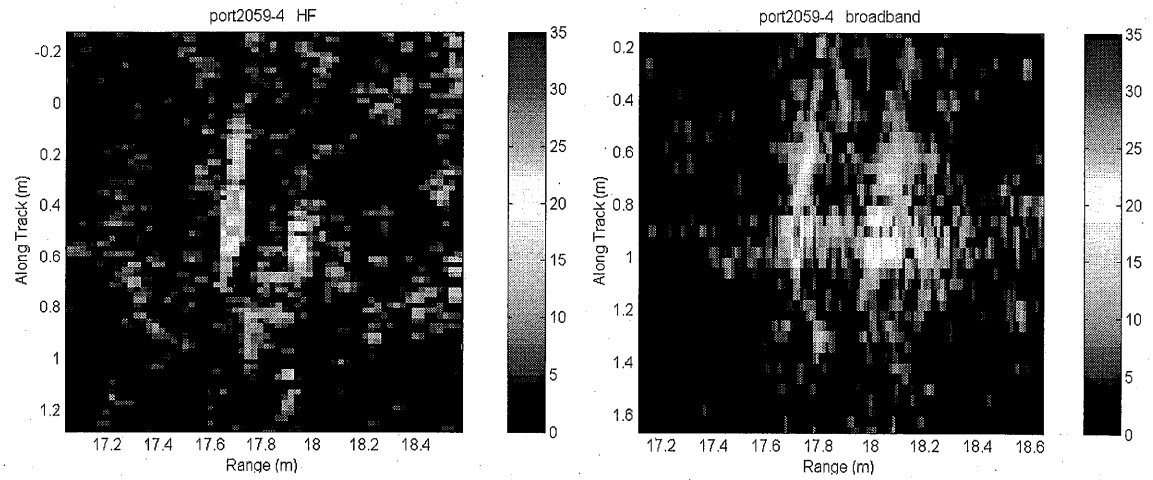

Fig. 7. High frequency and broadband end-on images of half-buried 5x25-cm cylinder.

Figure 7 shows the half-buried 5x25-cm cylinder in a similar end-on aspect. The detections are similar, but scaled down. The broadband image has a 30.2-dB SNR and the high frequency image has a 25.8-dB SNR. Again, the far end has the eyebolt attached by parachute cord to a buried screw anchor.

Two examples of broadside detections are shown in figures 8 and 9. The half-buried 15x70-cm cylinder is shown in figure 8. The diver's video shows a classic scouring pattern around this target that includes sand tending to mound around the mid portion of this target. This is exactly what the high frequency SAS image shows. The high frequency detection has a 41.3-dB SNR, and the broadband detection has a 39.6-dB SNR. The buried 7.5x35-cm cylinder is shown in figure 9 at just above the critical angle. The high frequency signal is very weak. The broadband detection has a 31.3-dB SNR. It is interesting that this image also clearly shows three additional returns close behind the spectral return. These are likely shell-coupled waves that decrease by about -4 dB, -8 dB, and -12 dB.

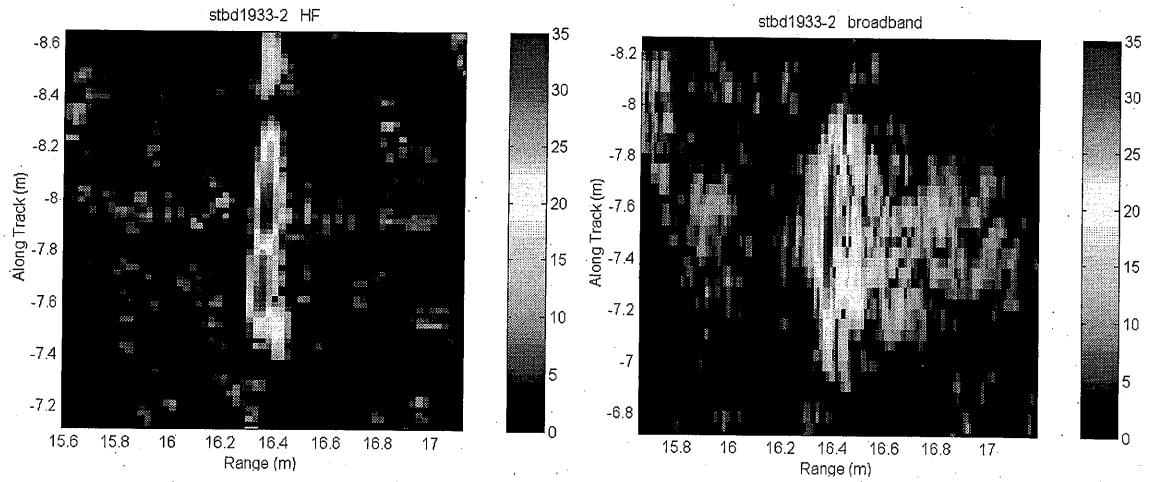

Fig. 8. High frequency and broadband end-on images of half-buried 15x70-cm cylinder.

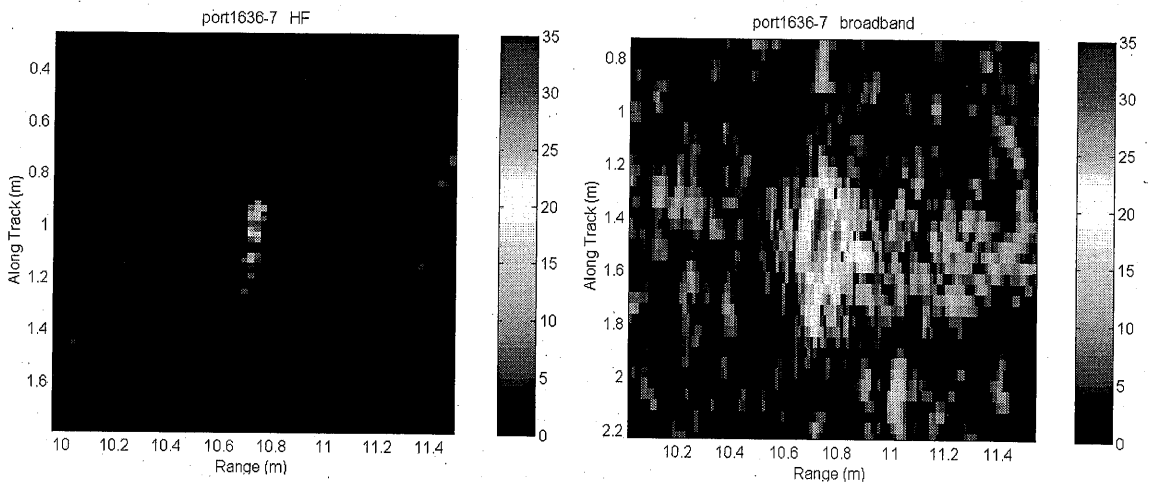

Fig. 9. High frequency and broadband end-on images of buried 7.5x35-cm cylinder.

It is worthwhile to compare the at-sea measured data to computer simulations. PCSWAT was used to investigate the end-on and broadside aspect cases. Figure 10 shows the result of a simulated 120 kHz image of an end-on aspect of a 60% buried 10x50-cm cylinder. PCSWAT yields a 47.6 dB signal peak, which compares to the measured at-sea SAS signal of 41.6 dB. The simulated image is more compact, especially in range, than the at-sea image. This is likely due to the Hamming filters used in the SAS beamformer. This type of filter tends to broaden signals, while greatly reducing sidelobe leakage. This explanation seems to be verified since the simulated image for this bright object shows a significant and extended sidelobe structure, which is only slightly seen in the at-sea data.

Figure 11 shows a PCSWAT generated broadband image of a near-broadside aspect of the buried 7.5x35-cm cylinder. The simulation assumed the target was buried 3-cm deep at an angle just above the critical angle. PCSWAT yielded a 31.6 dB signal peak, which compares favourably to the measured at-sea SAS signal of 31.7 dB. Again, the extended sidelobe structure seen in the simulation is not seen in the at-sea SAS image.

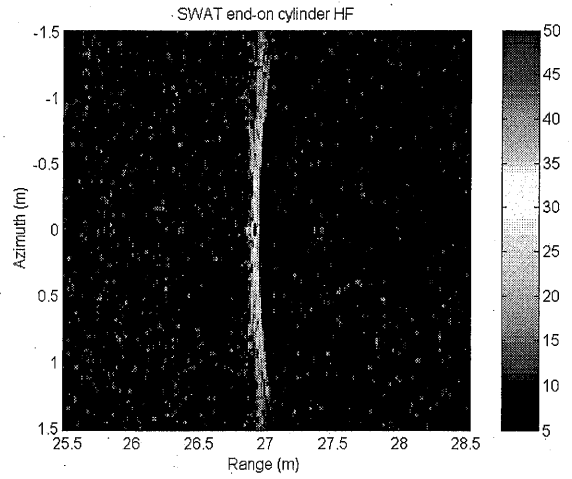

Fig. 10. Simulation of high frequency image.

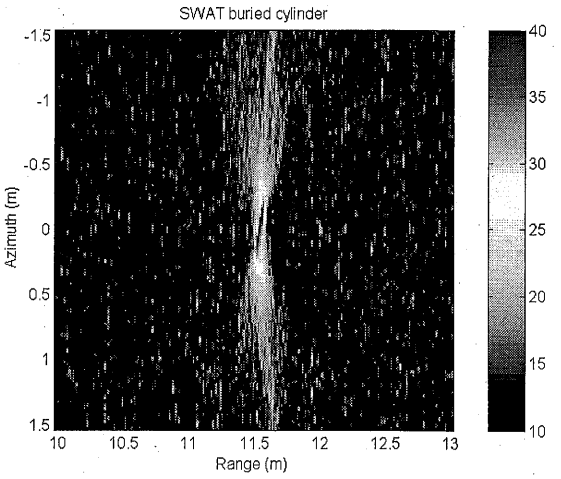

Fig. 11. Simulation of broadband image.

A complete listing of all the detections from broadside and end-on aspects is shown in figure 12. The signal-to-noise ratios were calculated by comparing the highest value pixel in the image to a nearby area mean value. Both broadside and end-on aspects are shown for both the broadband and the high frequency arrays. Additionally, the various target sizes and burial states are identified.

The detections generally fall between 25 and 40 dB. Target aspect to the sonar is important. Although the buried targets where close to being perpendicular or parallel to the runs, the proud targets were generally not. The D proud target was skewed about 45° and was not included in figure 12. The B proud target was also skewed and was just barely captured in the broadside broadband beampattern.

The data indicates that the end-on aspects from the eyebolt side were typically stronger. Also, the D buried target is the only target likely still fully buried. Although the divers did not see the B and C buried targets, they are likely not fully buried according to the data.

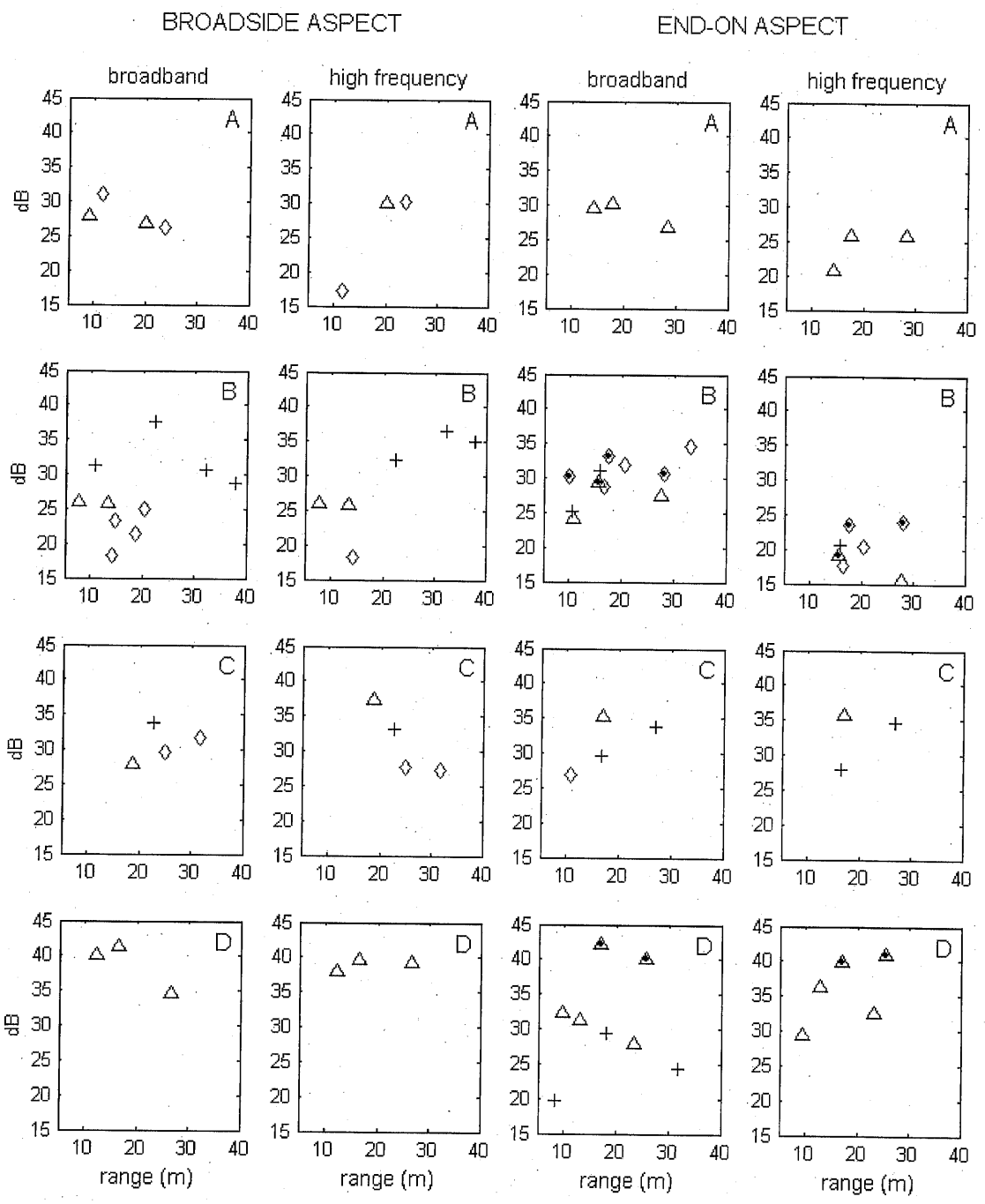

Fig. 12. Measured signal-to-noise ratios for the various targets. Pre-hurricane target dispositions are noted by diamonds (proud), triangles (half buried), and crosses (buried). The end-on aspects from the eyebolt and parachute cord end are indicated with a dot in the symbol. Target sizes from top to bottom are: (A) 5x25 cm, (B) 7.5x35 cm, (C) 10x50 cm, and (D) 15x70 cm.

5 COMMENTS

The targets used in this test were challenging because of their small size and burial states. SSAM proved to be a stable SAS platform during all the testing, and this led to consistently good imagery. Broadside and end-on aspects produced the best detections. Typically, these were at 25 to 40-dB signal strengths with the larger targets generally having the higher SNRs. Some variability in the individual target detections is seen and should be expected because of the near-Nyquist sampling and residual uncompensated motion. There does not seem to be a strong correlation with signal-to-noise ratios and range in the data, except at the very shortest ranges where the vertical beampattern of the sonar falls off it is difficult to get good detections.

Future work in small object detection will hopefully take place at underwater UXO sites. This will be a good test of SAS capabilities and serve an important mission.

6 ACKNOWLEDGEMENT

The authors would like to thank the Strategic Environmental Research and Development Program (SERDP) and the Office of Naval Research for their support.

7 REFERENCES

1. J.E. Piper, K.W. Commander, E.I. Thorsos, and K.L. Williams, 'Detection of buried targets using a synthetic aperture sonar', IEEE J. Oceanic Engineering, Vol. 27, 495-501. (July 2002)
2. G.S. Sammelman, 'Personal computer shallow water acoustic toolset (PCSWAT), version 9.0', NSWC, Panama City, FL. (2006)
3. D.W. Hawkins, 'Synthetic aperture imaging algorithms with application to wide bandwidth sonar', Ph.D., University of Canterbury, Christchurch, New Zealand. (1996)